Chirping and Sudden Excitation of Energetic-Particle-Driven Geodesic Acoustic Modes in a Large Helical Device Experiment

Hao Wang (王灏),[1,*] Yasushi Todo (藤堂泰),[1,2] Takeshi Ido (井戸毅),[1] and Yasuhiro Suzuki (鈴木康浩)[1,2]
[1]National Institute for Fusion Science, National Institutes of Natural Sciences, Toki 509-5292, Japan
[2]SOKENDAI (The Graduate University for Advanced Studies), Toki 509-5292, Japan

(Received 20 October 2017; revised manuscript received 24 January 2018; published 27 April 2018)

Energetic-particle-driven geodesic acoustic modes (EGAMs) observed in a Large Helical Device experiment are investigated using a hybrid simulation code for energetic particles interacting with a magnetohydrodynamic (MHD) fluid. The frequency chirping of the primary mode and the sudden excitation of the half-frequency secondary mode are reproduced for the first time with the hybrid simulation using the realistic physical condition and the three-dimensional equilibrium. Both EGAMs have global spatial profiles which are consistent with the experimental measurements. For the secondary mode, the bulk pressure perturbation and the energetic particle pressure perturbation cancel each other out, and thus the frequency is lower than the primary mode. It is found that the excitation of the secondary mode does not depend on the nonlinear MHD coupling. The secondary mode is excited by energetic particles that satisfy the linear and nonlinear resonance conditions, respectively, for the primary and secondary modes.

DOI: 10.1103/PhysRevLett.120.175001

The geodesic acoustic mode (GAM) is an oscillatory zonal flow coupled with density and pressure perturbations in toroidal plasmas [1–4]. In the last decade, energetic-particle-driven GAMs (EGAMs) were observed at the Joint European Torus [5,6], the DIII-D [7–9], the Large Helical Device (LHD) [10–14], and the ASDEX Upgrade [15]. In the DIII-D experiment, drops in neutron emission followed the EGAM bursts, suggesting beam ion losses [7]. Also, in the LHD experiment, anomalous bulk ion heating during the EGAM activity suggests a GAM channeling [12]. In addition, EGAM can interact with turbulence and affect the plasma confinement [16,17]. The understanding of the EGAM thus is important for magnetic confinement fusion where the energetic particles need to be well confined and the bulk plasma needs to be efficiently heated. The EGAM has been studied extensively. It was demonstrated that the poloidal mode number of the EGAM is $m = 0$ for potential and $m = 1$ for density. Also, the EGAM is a global mode with the spatially uniform oscillation frequency. In addition, the EGAM frequency can be lower or higher than the conventional GAM frequency under different conditions [18–21]. The above discussion has been advanced theoretically, computationally, and experimentally.

Recently, in LHD an abrupt excitation of a half-frequency secondary mode was observed when the frequency of a chirping primary EGAM reached twice the GAM frequency [14]. The secondary mode is important because of its low frequency. The lower frequency mode has a lower phase velocity; thus, this mode interacts more easily with the thermal ions and transfers energy to ions. As a result, the plasma heating thus becomes easier. Since the appearance of the secondary mode is related to the neutral beam injection (NBI), the secondary mode may create an energy channel between the energetic particles and the bulk plasmas. A one-dimensional simulation with the kinetic energetic particles and a nonlinear coupling coefficient between the primary and secondary modes was used to reproduce these two modes [22]. Lesur *et al.* [22] have claimed that the secondary mode is driven by the cooperative combination of fluid nonlinearity and kinetic nonlinearity.

MEGA [23–25], a hybrid simulation code for energetic particles interacting with a magnetohydrodynamic (MHD) fluid, is used for the simulation of EGAMs. In the MEGA code, the bulk plasma is described by the nonlinear MHD equations. The drift kinetic description and the δf particle method are applied to the energetic particles.

A realistic three-dimensional equilibrium generated by HINT code [26] is used for the simulation. These equilibrium data are based on the LHD shot No. 109031 at time $t = 4.94$ s . At that time, $t = 4.94$ s, the EGAM activity is very strong; thus, it is appropriate to reproduce the EGAM phenomenon in a simulation.

In the experiments of LHD, the EGAMs were observed under the bump-on-tail energetic particle distribution [12,14]. Thus, in this Letter, we implement the simulation with the same type of distribution. For the bump-on-tail distribution, the charge exchange is considered, and the velocity distribution is

$$f(v) = C(v^3 + v_c^3)^{(1/3)\tau_s/\tau_{cx}-1}, \tag{1}$$

which is the same as Eq. (1) in Ref. [21]. C is an integration constant, v_c is the critical velocity, τ_s is the slowing-down

 © 2018 American Physical Society

time, and τ_{cx} is the charge exchange time. The shape of the distribution function is controlled by the ratio τ_s/τ_{cx}. For $\tau_{cx} \to \infty$, the τ ratio is 0 and the distribution function is the typical slowing-down type. With the increase of τ_s/τ_{cx}, the slowing down becomes insufficient gradually, and more energetic particles distribute in the high-energy region and form a bump-on-tail distribution. The distribution function of $f(v)$ in this Letter is the same as the experimental observations [13,14].

In addition, a Gaussian-type pitch angle distribution $g(\Lambda)$ is assumed for the energetic ions:

$$g(\Lambda) = \exp[-(\Lambda - \Lambda_{\text{peak}})^2/\Delta\Lambda^2], \tag{2}$$

where Λ_{peak} represents the pitch angle for the distribution peak and $\Delta\Lambda$ is a parameter to control the distribution width.

The parameters for the EGAM simulation are based on a LHD experiment [14]. Those parameters are $B_0 = 1.5$ T, electron density $n_e = 0.1 \times 10^{19}$ m^{-3}, electron temperature at the magnetic axis $T_e = 4$ keV, and bulk plasma β value on the magnetic axis equal to 7.2×10^{-4}. The counter-injected neutral beam energy is $E_{\text{NBI}} = 175$ keV. The safety factor q profile is negative normal shear with the value 2.82 at the magnetic axis and 0.84 at the plasma edge. The major radius of the magnetic axis is $R_0 = 3.7$ m. Cylindrical coordinates (R, ϕ, z) are employed. For LHD equilibrium, there are ten pitches in the toroidal direction. Since the toroidal mode number of the GAM is $n = 0$, for simplicity, only one pitch from $\phi = 0$ to $\phi = 0.2\pi$ is used for the present simulation, while other pitches from $\phi = 0.2\pi$ to $\phi = 2\pi$ are obtained by periodic extension. This simplification is made to save computational resources and time. The numbers of grid points of this pitch in the (R, ϕ, z) directions are (128,64,128), respectively.

Both the chirping primary mode and the half-frequency secondary mode are reproduced with the MEGA code, as shown in Fig. 1. Figure 1(a) shows the poloidal velocity v_θ frequency spectrum including all of the frequency components, and Fig. 1(b) shows v_θ evolution including only 50 and 100 kHz components. The primary mode frequency chirps up in the nonlinear phase from 70 kHz in the linear growth phase. The mode is saturated at $t = 0.07$ ms and then moves into the nonlinear phase. At $t = 1.7$ ms, the frequency of the primary mode reaches 102 kHz, and a secondary mode with frequency $f = 51$ kHz is excited. The amplitudes of the primary mode and the secondary mode are close to each other. The simulated phenomenon is very similar to the experimental observation, as shown in Fig. 2 of Ref. [14]. This is the first simulation that reproduces both the primary mode and the secondary mode with a three-dimensional model and realistic input parameters.

The frequency of the primary mode is 2 times that of the secondary mode, and this frequency relation can be easily confirmed by Lissajous curves. Figure 2 shows the Lissajous curves between dB_θ/dt associated with the primary and secondary modes. Figure 2(a) is plotted in the growth phase and Fig. 2(b) is plotted in the decay phase of the secondary mode. The phase locking is clearly shown in the figure, and it indicates a coupling between the primary mode and the secondary mode. The Lissajous curves in the present simulation are consistent with the experiments, as shown in Fig. 5 of Ref. [14].

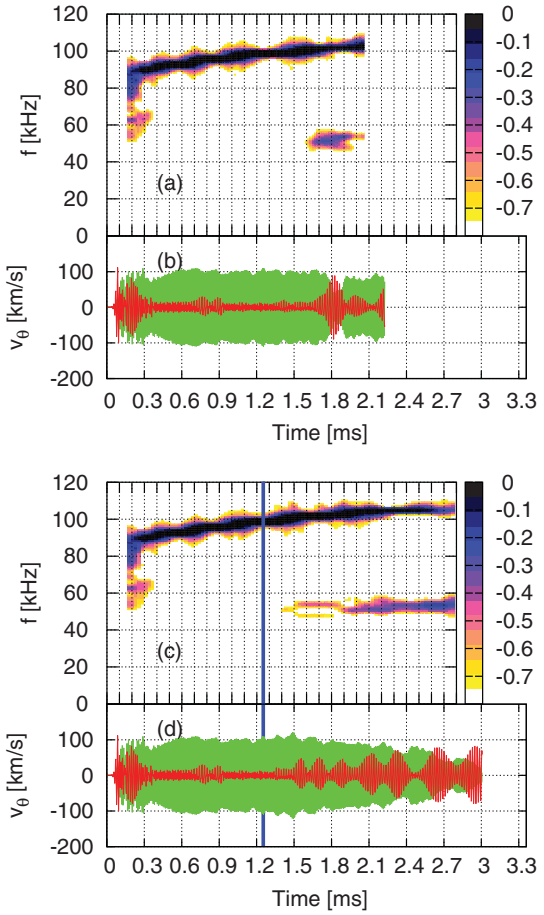

FIG. 1. The EGAMs in LHD are reproduced by MEGA code. (a) The poloidal velocity frequency spectrum including all of the frequency components. (b) The poloidal velocity time evolution including only 50 kHz (red) and 100 kHz (green). (c) and (d) are similar to (a) and (b), but the MHD equations are linearized from $t = 1.253$ ms.

The mode profiles of poloidal velocity v_θ and bulk pressure perturbation δP_{bulk} are plotted in three-dimensional figures, as shown in Fig. 3. The five slices in each panel represent five poloidal cross sections, and their toroidal positions are from $\phi = 0$ to $\phi = 0.4\pi$, with a toroidal interval of 0.1π. For v_θ, red represents a positive value. In other words, red represents counterclockwise rotation in the poloidal direction, while blue represents clockwise rotation. For δP_{bulk}, red represents positive perturbation, while blue represents negative perturbation.

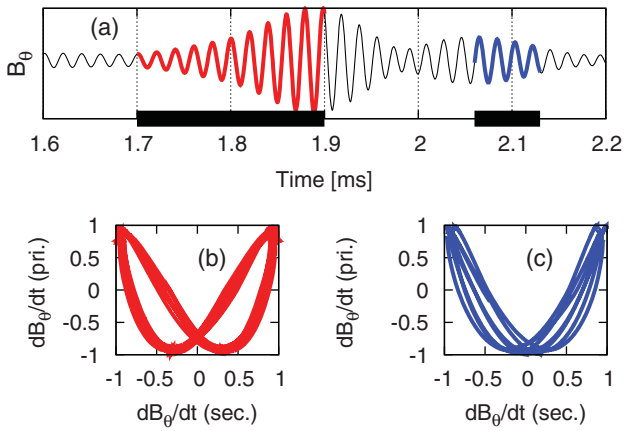

FIG. 2. Lissajous curves between dB_θ/dt values associated with the primary and secondary modes. (a) represents the time evolution of the secondary mode, while (b) and (c) correspond to the Lissajous curves in the growth phase (red) and the decay phase (blue), respectively.

Figure 3 shows that the dominant components of v_θ and δP_{bulk} are $m/n = 0/0$ and $1/0$, respectively. Also, further analyses show that both the primary mode and the secondary mode are global. The mode number and the mode structure are consistent with the experiment, as shown in Fig. 4 of Ref. [14].

The poloidal velocity v_θ is a combination of $m/n = 0/0$ (strong), $1/0$ (medium), and $2/10$ (weak) components. The $m/n = 2/10$ component exists due to the LHD configuration, because in the LHD there are ten pitches in the toroidal direction and there are two high field regions and two low field regions in the poloidal direction. This is the first simulation of EGAM in the three-dimensional LHD configuration. The mode number is different from the tokamak case where the v_θ oscillation is a combination of the $m/n = 0/0$ and $1/0$ components.

The secondary mode is identified as an EGAM in this Letter for three reasons. First, the poloidal mode number is $m = 0$ for poloidal velocity and $m = 1$ for pressure perturbation. This is the feature of the EGAM and the conventional GAM. Second, the mode frequency is almost the same as the conventional GAM frequency. According to

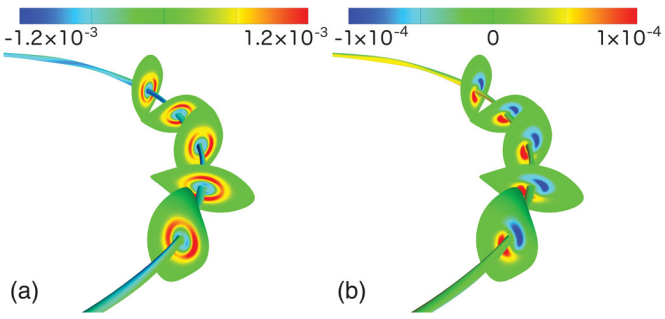

FIG. 3. The mode profiles of (a) v_θ and (b) δP_{bulk} in the three-dimensional form.

the theoretical prediction, under the present simulation conditions, the conventional GAM frequency should be 50.1 kHz. The simulated frequency of the secondary mode is 51 ± 1.5 kHz. And third, the secondary mode is global. The EGAM is global, while the conventional GAM is local. This is one of the differences between the EGAM and the conventional GAM [7,15,18,20]. The global structure is caused by the large energetic particle orbit width [8,9,15,18,20]. The coupling strength between the energetic particles and the conventional GAM changes by bulk plasma temperature and GAM continuum, and thus the mode structure can also be affected by bulk plasma [4,15,19]. Based on the three properties discussed above, we conclude that the simulated secondary mode is an EGAM. A question may arise regarding why the primary EGAM and the secondary EGAM have different frequencies. In order to clarify the reason, the bulk plasma pressure perturbation δP_{bulk} and the energetic particle pressure perturbation $\delta P_{h\parallel}$ are analyzed, as shown in Fig. 4. The most dominant component of δP_{bulk} and $\delta P_{h\parallel}$ is $m/n = 1/0$ sine. For simplicity, only this dominant component $1/0$ sine is shown in Fig. 4. For the primary mode, the phase of δP_{bulk} and $\delta P_{h\parallel}$ are the same, and they enhance each other. The primary mode is driven by both δP_{bulk} and $\delta P_{h\parallel}$. For the secondary mode, the phase difference between δP_{bulk} and $\delta P_{h\parallel}$ is π. In other words, they are in antiphase, and they cancel each other out. Thus, the frequency of the secondary mode is much lower than the primary mode. The phase of $\delta P_{h\perp}$ is the same as $\delta P_{h\parallel}$, but the absolute value of $\delta P_{h\perp}$ is much smaller. Thus, $\delta P_{h\perp}$ is not shown in the figure.

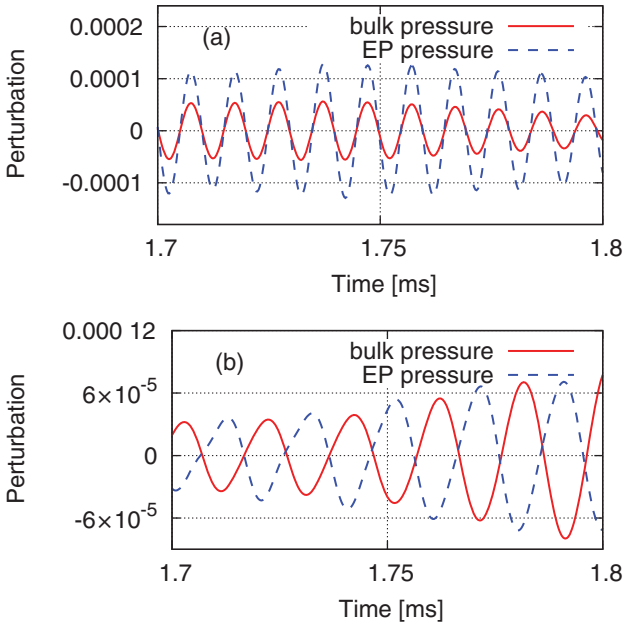

FIG. 4. The δP_{bulk} oscillation and the $\delta P_{h\parallel}$ oscillation of (a) the primary mode and (b) the secondary mode. EP is the abbreviation of energetic particle.

In Ref. [22], the authors claimed that both the fluid nonlinearity and the kinetic nonlinearity are important for the secondary mode excitation. In order to clarify the importance of the fluid nonlinearity, a special linearized MHD model is applied in this Letter. The linear MHD equations are the same as those in Ref. [23]. In this work, simulations are performed in two stages. In the first stage, the nonlinear code is run until time $t = 1.253$ ms, when the EGAM is completely saturated but the secondary mode has not yet been excited. Then, in the second stage, both the linear and the nonlinear MHD codes are run separately from the end of the run of the first stage. In the second stage, the secondary mode appears in both runs. In other words, the secondary mode can be excited even if the MHD equations are linearized. In the linearized MHD run, the appearance of the secondary mode is delayed, but the amplitude is almost the same. This result is different from that in Ref. [22]. In this work, the excitation of the secondary mode is only caused by the kinetic nonlinearity, while the fluid nonlinearity hardly affects the amplitude of the secondary mode.

In order to determine the reason why the frequency relation between the primary mode and the secondary mode is exactly double that which is shown in Fig. 2, and also to further confirm the role of the kinetic nonlinearity, the energy transfer versus transit frequencies of resonant particles is plotted in Fig. 5. Three lines correspond to different phases of the secondary mode: before the excitation, during the growth, and at the time of the beginning of decay at maximum amplitude. The poloidal transit frequency is defined by $f_{\rm tr} = \sqrt{(1-\Lambda)(2E/m_{\rm EP})}/(2\pi q R_0)$, where $m_{\rm EP}$ is the energetic particle mass. The negative dE/dt indicates that the energetic particles lose energy and the energy is transferred to the mode, and thus the mode is destabilized. We see in Fig. 5 that the energy transfer is strong when the secondary mode is growing at $t = 1.75$ ms. This indicates that the energy transfer from the particles with $f_{\rm tr} \approx 100$ kHz excited the secondary mode with $f \approx 50$ kHz. This interaction may be the nonlinear resonance. For the linear resonance, the phase of the wave is the same when the particle passes each time around the poloidal angle [27], while the phase is the same when the particle passes K ($K > 1$) times around the poloidal angle for the nonlinear resonance. The nonlinear resonance is negligible for the linear stability analysis but may transfer substantial energy for finite-amplitude waves. Nonlinear resonance is also called higher-order resonance or fractional resonance, and it is commonly known [28]. Fractional resonances were demonstrated experimentally and computationally for EGAMs [8,21]. For the excitation of the secondary mode shown in Fig. 1, the particles with $f_{\rm tr} \approx 100$ kHz satisfy the linear resonance condition for the primary mode with $f \approx 100$ kHz and the nonlinear resonance condition for the secondary mode with $f \approx 50$ kHz and $K = 2$. These resonant particles may transfer energy from the primary mode to the secondary mode, which can be inferred from the decay of the primary mode when the secondary mode is excited.

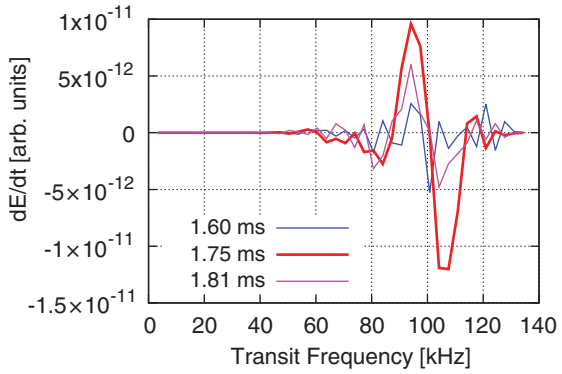

FIG. 5. The energy transfer versus transit frequencies of resonant particles at 1.60, 1.75, and 1.81 ms.

In summary, three conclusions are presented in this Letter. First, the simulation of EGAM in the realistic three-dimensional equilibrium is obtained for the first time, and the results are very similar to the experimental observation. It is found that the poloidal velocity oscillation is a combination of $m/n = 0/0$ (strong), $1/0$ (medium), and $2/10$ (weak) components. This is caused by the LHD configuration and is different than the tokamak case. Second, the chirping EGAM and the associated half-frequency secondary mode are reproduced with the three-dimensional model and realistic parameters for the first time. The results are good validations of the simulation. It is found that the phase difference between $\delta P_{\rm bulk}$ and $\delta P_{h\|}$ is π for the secondary mode. The $\delta P_{\rm bulk}$ and $\delta P_{h\|}$ are in antiphase, and they cancel each other out. Thus, the frequency of the secondary mode is much lower than the primary mode. And third, it is found that the fluid nonlinearity does not affect the excitation of the secondary mode, and the secondary mode is excited by the energetic particles that can resonate with both the primary and secondary modes. This conclusion is confirmed by the linearized MHD run and by the analysis of the energy transfer from energetic particles to the mode. Our conclusion is different from that of Ref. [22]. However, we would like to emphasize that our simulations are based on the fundamental physics equations with the realistic condition.

We have found that the secondary mode is excited by energetic particles that satisfy both the linear and nonlinear resonance conditions for the primary and secondary modes, respectively. The overlap of linear and nonlinear resonances is brought about by the spontaneous frequency chirping of the primary mode, and it leads to the emergence of stochasticity and the sudden excitation of the secondary mode. The overlap of linear and nonlinear resonances can be ubiquitous in fusion plasmas and important for plasma confinement and energy channeling.

Numerical computations were performed on the Plasma Simulator of NIFS with the support and under the auspices

of the NIFS Collaboration Research program (NIFS17KNST111), the Helios of the International Fusion Energy Center, and the K Computer of the RIKEN Advanced Institute for Computational Science (Project No. hp170260). This work was partly supported by MEXT as "Priority Issue on Post-K computer" (Accelerated Development of Innovative Clean Energy Systems) and the JSPS-NRF-NSFC A3 Foresight Program in the field of Plasma Physics (NRF Grant No. 2012K2A2A6000443, NSFC Grant No. 11261140328). The authors thank Professor M. Osakabe, Professor H. Sugama, Professor Y. Idomura, Professor M. Yokoyama, Dr. M. Lesur, Professor G. Fu, and Professor W. Chen for the fruitful discussions.

*wanghao@nifs.ac.jp

[1] N. Winsor, J. L. Johnson, and J. M. Dawson, Phys. Fluids **11**, 2448 (1968).
[2] P. H. Diamond, S.-I. Itoh, K. Itoh, and T. S. Hahm, Plasma Phys. Controlled Fusion **47**, R35 (2005).
[3] H. Sugama and T.-H. Watanabe, Phys. Plasmas **13**, 012501 (2006).
[4] F. Zonca and L. Chen, Europhys. Lett. **83**, 35001 (2008).
[5] C. Boswell, H. Berk, D. Borba, T. Johnson, S. Pinches, and S. Sharapov, Phys. Lett. A **358**, 154 (2006).
[6] H. Berk, C. Boswell, D. Borba, A. Figueiredo, T. Johnson, M. Nave, S. Pinches, S. Sharapov, and JET EFDA contributors, Nucl. Fusion **46**, S888 (2006).
[7] R. Nazikian, G. Y. Fu, M. E. Austin, H. L. Berk, R. V. Budny, N. N. Gorelenkov, W. W. Heidbrink, C. T. Holcomb, G. J. Kramer, G. R. McKee, M. A. Makowski, W. M. Solomon, M. Shafer, E. J. Strait, and M. A. Van Zeeland, Phys. Rev. Lett. **101**, 185001 (2008).
[8] G. J. Kramer, L. Chen, R. K. Fisher, W. W. Heidbrink, R. Nazikian, D. C. Pace, and M. A. Van Zeeland, Phys. Rev. Lett. **109**, 035003 (2012).
[9] R. K. Fisher, D. C. Pace, G. J. Kramer, M. A. Van Zeeland, R. Nazikian, W. W. Heidbrink, and M. Garcia-Munoz, Nucl. Fusion **52**, 123015 (2012).
[10] K. Toi *et al.*, Phys. Rev. Lett. **105**, 145003 (2010).
[11] T. Ido *et al.*, Nucl. Fusion **51**, 073046 (2011).
[12] M. Osakabe, T. Ido, K. Ogawa, A. Shimizu, M. Yokoyama, R. Seki, C. Suzuki, M. Isobe, K. Toi, D. A. Spong, K. Nagaoka, Y. Takeiri, H. Igami, T. Seki, K. Nagasaki, and the LHD Experiment Group, in *Proceedings of the 25th IAEA Fusion Energy Conference, St. Petersburg, Russia, 2014* (IAEA, Trieste, 2014), http://www-naweb.iaea.org/napc/physics/FEC/FEC2014/fec_sourcebook_online.pdf.
[13] T. Ido, M. Osakabe, A. Shimizu, T. Watari, M. Nishiura, K. Toi, K. Ogawa, K. Itoh, I. Yamada, R. Yasuhara, Y. Yoshimura, S. Kato, and the LHD Experiment Group, Nucl. Fusion **55**, 083024 (2015).
[14] T. Ido, K. Itoh, M. Osakabe, M. Lesur, A. Shimizu, K. Ogawa, K. Toi, M. Nishiura, S. Kato, M. Sasaki, K. Ida, S. Inagaki, S.-I. Itoh, and the LHD Experiment Group, Phys. Rev. Lett. **116**, 015002 (2016).
[15] L. Horvath, G. Papp, Ph. Lauber, G. Por, A. Gude, V. Igochine, B. Geiger, M. Maraschek, L. Guimarais, V. Nikolaeva, G. I. Pokol, and the ASDEX Upgrade Team, Nucl. Fusion **56**, 112003 (2016).
[16] D. Zarzoso, Y. Sarazin, X. Garbet, R. Dumont, A. Strugarek, J. Abiteboul, T. Cartier-Michaud, G. Dif-Pradalier, Ph. Ghendrih, V. Grandgirard, G. Latu, C. Passeron, and O. Thomine, Phys. Rev. Lett. **110**, 125002 (2013).
[17] M. Sasaki, K. Itoh, K. Hallatschek, N. Kasuya, M. Lesur, Y. Kosuga, and S.-I. Itoh, Sci. Rep. **7**, 16767 (2017).
[18] G. Y. Fu, Phys. Rev. Lett. **101**, 185002 (2008).
[19] Z. Qiu, F. Zonca, and L. Chen, Plasma Sci. Technol. **13**, 257 (2011).
[20] H. Wang and Y. Todo, Phys. Plasmas **20**, 012506 (2013).
[21] H. Wang, Y. Todo, T. Ido, and M. Osakabe, Phys. Plasmas **22**, 092507 (2015).
[22] M. Lesur, K. Itoh, T. Ido, M. Osakabe, K. Ogawa, A. Shimizu, M. Sasaki, K. Ida, S. Inagaki, S.-I. Itoh, and the LHD Experiment Group, Phys. Rev. Lett. **116**, 015003 (2016).
[23] Y. Todo, H. Berk, and B. Breizman, Nucl. Fusion **50**, 084016 (2010).
[24] H. Wang, Y. Todo, and C. C. Kim, Phys. Rev. Lett. **110**, 155006 (2013).
[25] Y. Todo, R. Seki, D. A. Spong, H. Wang, Y. Suzuki, S. Yamamoto, N. Nakajima, and M. Osakabe, Phys. Plasmas **24**, 081203 (2017).
[26] Y. Suzuki, N. Nakajima, K. Watanabe, Y. Nakamura, and T. Hayashi, Nucl. Fusion **46**, L19 (2006).
[27] Y. Todo and T. Sato, Phys. Plasmas **5**, 1321 (1998).
[28] G. J. Lewak and C. S. Chen, J. Plasma Phys. **3**, 481 (1969).